Anatomical organization of forward fiber projections from area TE to perirhinal neurons representing visual long-term memory in monkeys

Masatoshi Yoshida*, Yuji Naya*, and Yasushi Miyashita†

Department of Physiology, University of Tokyo School of Medicine, Hongo, Tokyo 113-0033, Japan; and Laboratory of Cognitive Neuroscience, National Institute for Physiological Sciences, Okazaki, Aichi 444-8585, Japan

A number of studies have shown that the perirhinal (PRh) cortex, which is part of the medial temporal lobe memory system, plays an important role in declarative long-term memory. The PRh cortex contains neurons that represent visual long-term memory. The aim of the present study is to characterize the anatomical organization of forward projections that mediate information flow from visual area TE to memory neurons in the PRh cortex. In monkeys performing a visual pair-association memory task, we conducted an extensive mapping of neuronal responses in the anteroventral part of area TE (TEav) and area 36 (A36) of the PRh cortex. Then, three retrograde tracers were separately injected into A36 and the distribution of retrograde labels in TEav was analyzed. We focused on the degree of divergent projections from TEav to memory neurons in A36, because the highly divergent nature of these forward fiber projections has been implicated in memory function. We found that the degree of divergent projection to memory neurons in A36 was smaller from the TEav neurons selective to learned pictures than from the nonselective TEav neurons. This result demonstrates that the anatomical difference (the divergence) correlates with the physiological difference (selectivity of TEav neurons to the learned pictures). Because the physiological difference is attributed to whether the projections are involved in information transmission required for memory neurons in A36, it can be speculated that the reduced divergent projection resulted from acquisition of visual long-term memory, possibly through retraction of the projecting axon collaterals.

It has been recognized that the perirhinal (PRh) cortex, which is part of the memory system in the medial temporal lobe (1), plays a critical role in declarative long-term memory (1, 2). Lesions in the PRh cortex of macaque monkeys impair the formation of recognition memory (3, 4) and stimulus–stimulus association memory (5). There is a double dissociation between the effects of a lesion to the PRh cortex and those of lesions to area TE, which is a visual-association cortex immediately adjacent to the PRh cortex (6, 7). Single-unit studies show that responses of PRh neurons represent visual-associative long-term memory during (8) and after (9, 10) learning. Recently, we reported that the degree of memory coding in PRh neurons was much higher than in TE neurons, which provided evidence that forward signal transmission from area TE to the PRh cortex is the critical step from visual to mnemonic processing, suggesting contributions of several long-term plasticity mechanisms for the critical step (11). In the present study, we sought an anatomical correlate of the plasticity mechanisms. The anteroventral part of area TE (TEav) sends dense and highly divergent fibers to area 36 (A36) of the PRh cortex (12, 13). The highly divergent nature of this projection has been implicated in memory function (12, 13). Thus, we focused on the degree of divergent projection from TEav to memory-related neurons in A36.

The experimental design is illustrated in Fig. 1. In monkeys that were extensively trained in a visual pair-association memory task (9, 14), we recorded neuronal responses to learned pictures in A36 and TEav (Fig. 1 *Left*). As expected from previous

findings (9–11), neurons selective to learned pictures were localized in a focal patch in A36 (hotspot; Fig. 1 *Left*; see also Fig. 2) and they indeed coded visual long-term memory. In a tracer injection study, then (Fig. 1 *Right*), a retrograde tracer was injected into the hotspot (hotspot injection) and two different kinds of tracer were injected as control (control injection). By combining anatomical and electrophysiological data, the degree of divergent projection from TEav neurons to the hotspot in A36 was compared between neurons involved (picture-selective neurons) and those not involved (nonselective neurons) in task-related visual processing (Fig. 1 *Right*). Experiments were carefully designed to control the effect of the difference between monkeys by using a within-animal comparison paradigm. The advantage of this experimental design is that it enhances the power to detect differences in anatomical measures and it greatly reduces the problem arising from using different tracers.

Methods

Behavioral Task and Electrophysiology. All experiments were conducted in accordance with the National Institutes of Health Guide for the Care and Use of Laboratory Animals, and with the regulations of the National Institute for Physiological Sciences of Japan. Three adult monkeys (*Macaca fuscata*; 6.0–9.0 kg) were trained with a pair-association task using 24 monochrome Fourier descriptors (15, 16). The duration of experience that each animal had with the stimulus set before the beginning of recording sessions was 3.5 months in monkey A, 3 months in monkey B, and 4 months in monkey C. The duration of recording in each animal was 12 months in monkey A, 10 months in monkey B, and 14 months in monkey C. Single-unit recording was performed as described (16). The three animals in the present study were also used in our previous electrophysiological study of the inferior temporal cortex (11, 16). The recorded neurons in A36 and in TEav were classified as picture-selective or nonselective, based on the response during the cue period (60–320 ms after the cue onset, ANOVA, $P < 0.01$; ref. 16). The location of the electrode track for each recording session was measured on an x-ray image (14, 17). See *Supporting Methods*, which is published as supporting information on the PNAS web site, www.pnas.org, for evaluation of measurement error.

Triple Injection and Histology. After the electrophysiological identification of the hotspot in A36, three different retrograde tracers [fast blue (FB; Sigma), 3%, 150–180 nl; diamidino yellow (DY; Sigma), 2%, 280–450 nl; and cholera toxin B subunit (CTB; List Biological Laboratories, Campbell, CA), 10%, 100 nl]
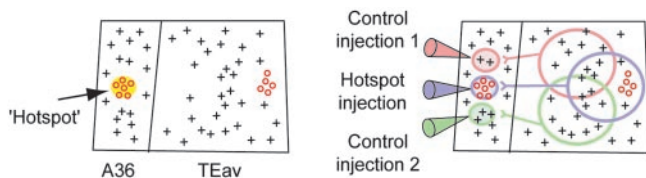
NEUROSCIENCE

Fig. 1. The experimental design. (*Left*) Single-unit recording. We conducted an extensive mapping of neuronal responses in A36 and TEav. Recorded neurons were classified into picture-selective neurons (red circles) and non-selective neurons (gray crosses). The picture-selective neurons in A36 were localized in the hotspot (yellow). (*Right*) Injection of retrograde tracers. Retrograde tracers were injected into the hotspot (hotspot injection) and adjacent control regions (control injections 1 and 2) in A36. Then, the distribution of retrograde labels in TEav was compared with the distribution of recorded neurons.

were injected separately into the hotspot and the two control sites (18). The combination of injection sites and tracers in three monkeys was as follows: Monkey A: control 1, CTB; hotspot, FB; and control 2, DY. Monkey B: control 1, DY; hotspot, FB; and control 2, CTB. Monkey C: control 1, CTB; hotspot, FB; and control 2, DY. The total numbers of retrograde labels in area TE were 19,158, 16,180, and 39,205 (FB), 30,160, 33,641, and 14,091 (DY), and 18,699, 35,478, and 23,937 (CTB) in monkeys A, B, and C, respectively. There was no statistically significant difference in the number of retrograde labels between tracers ($F < 1$, repeated measures ANOVA). The tracers were injected through a glass micropipette containing a tungsten electrode. The target location for injection was identified by recording neuronal activity with the electrode in the pipette and by measuring the position of the electrode by x-ray imaging. This procedure enabled us to confine the injected tracers to the gray matter of the target that was determined by the prior single-unit recording.

Fourteen days after the FB and DY injection and 7 days after the CTB injection, the monkeys were perfused with 4% para-formaldehyde in phosphate buffer (pH 7.4). The brains were cut into 50 μm-thick coronal sections. One of every eight sections was used for data analysis. CTB was visualized by immunohistochemistry (19). The position of neurons labeled by the retrograde tracers (retrograde labels) was plotted with a computerized microscope system (KS400, Zeiss). The cytoarchitectonic borders were determined according to previous studies (12, 13). There is a clear separation between layer 5 and layer 6 in TEav but not in A36. Layer 2 of A36 is thinner than that of TEav and contains patches of darkly stained cells. Layer 5 is less populated by neurons in the anterodorsal part of area TE than in TEav. The extent of the tracers' uptake was determined according to the literature (19, 20).

Construction of Two-Dimensional Unfolded Map. A flat map of retrograde labels was constructed according to a previous paper (12). The gray matter was subdivided into rectangular regions (pixels) along layer 4 with a width of 250 μm. The number of the retrograde labels was counted in each pixel. The count was normalized by the area of the pixel and converted to a density value that was expressed as the number of labeled neurons per the average area of TE pixels. These procedures produced arrays of density values for each histological section. The arrays were then aligned section by section so that histological markers (e.g., border and sulcus) connected smoothly and the region of interest (ROI; either A36 in Fig. 2 or TEav in Figs. 4 and 5) was aligned with the minimum distortion.

A flat map of single-unit recordings was constructed in the same manner as that of the retrograde labels. The recording sites were histologically reconstructed from x-ray images (14, 16) based on three or four electrolytic lesions and three injected

dyes. Shrinkage of histological sections (7–15%) was corrected. See *Supporting Methods* for evaluation of measurement error.

Data Analysis. The results of this study consist of four data sets: single-unit recording in A36 and in TEav, anatomy of A36 (tracer injection), and TEav (retrograde labels). The main purpose of data analysis is to compare the distribution of retrograde labels in TEav with that of single-unit recording in TEav.

A hotspot was defined as a region with a statistically significant percentage of picture-selective neurons, based on Kulldorff's procedure (21, 22). Clusters of retrograde labels were statistically defined in each map (three monkeys × three injections). See *Supporting Methods* for further details.

In the ROI-based analysis, the percentage of picture-selective neurons in each ROI was calculated by using the following expression: [number of picture-selective neurons in the ROI/ {(number of picture-selective neurons in the ROI) + (number of nonselective neurons in the ROI)}] × 100. Their difference between ROIs was tested by the Cochran–Mantel–Haenszel (CMH) test (FREQ procedure in SAS; ref. 23), which is an extended version of the χ^2 test. Its test statistics uses the number of sampled picture-selective and nonselective neurons. See *Supporting Methods* for an accurate formula of CMH test statistics.

A map of the percentage of picture-selective neurons per pixel (Fig. 5b *Center*) was constructed as follows: A map of the number of picture-selective neurons in each pixel and a map of nonselective neurons in each pixel were constructed. Both maps were separately smoothed with a Gaussian kernel ($\sigma = 500$ μm). A map of the percentage of picture-selective neurons per pixel was obtained as [the smoothed map of picture-selective neurons per pixel/{(the smoothed map of picture-selective neurons per pixel) + (the smoothed map of nonselective neurons per pixel)}] × 100.

The divergence index (DI) in each pixel on the map was defined as the ratio of the amount of projections to the hotspot injection site (y_2) to the total amount of projections to three injection sites ($y_1 + y_2 + y_3$; Fig. 5a). Note that when the DI analysis was made on the neurons in the cluster of neurons labeled by injection to the hotspot, y_2 was always sufficiently larger than zero and the denominator of DI ($= y_1 + y_2 + y_3$) can never be zero or near to zero. DI was also calculated with normalization in which the total number of retrograde labels was the same among the three tracers. The DI analysis is based on the distribution of labeled neurons on the equally spaced histological sections throughout area TE.

Results

A Hotspot in A36. In 510 neurons recorded in A36 of three monkeys, 85 were responsive and 76 showed selective response to the learned pictures during cue presentation (ANOVA, $P < 0.01$; Fig. 2; ref. 11). As demonstrated in a coronal section, A36 picture-selective neurons (red circle) were aggregated (Fig. 2c *Left*; monkey A). Two-dimensional unfolded maps of single-unit recording (Fig. 2d) revealed that most of A36 picture-selective neurons were localized in a focal patch (the hotspot; see *Methods* and *Supporting Methods*) in each monkey. The degree of memory coding in the A36 hotspot, quantified by using the correlation coefficient between the cue responses to the paired pictures (9, 14), was markedly larger than zero (median = 0.52, $P < 10^{-8}$, Wilcoxon signed-rank test; $n = 60$; ref. 11). This result demonstrates that the picture-selective neurons in the A36 hotspot showed a strong memory-coding effect.

Triple Injection of Retrograde Tracers into A36. After the single-unit recording, three tracers (FB, DY, and CTB) were injected into three regions in A36 (Fig. 2 a and b). Injections were targeted to the hotspot and rostrocaudally adjacent control regions. Injec-
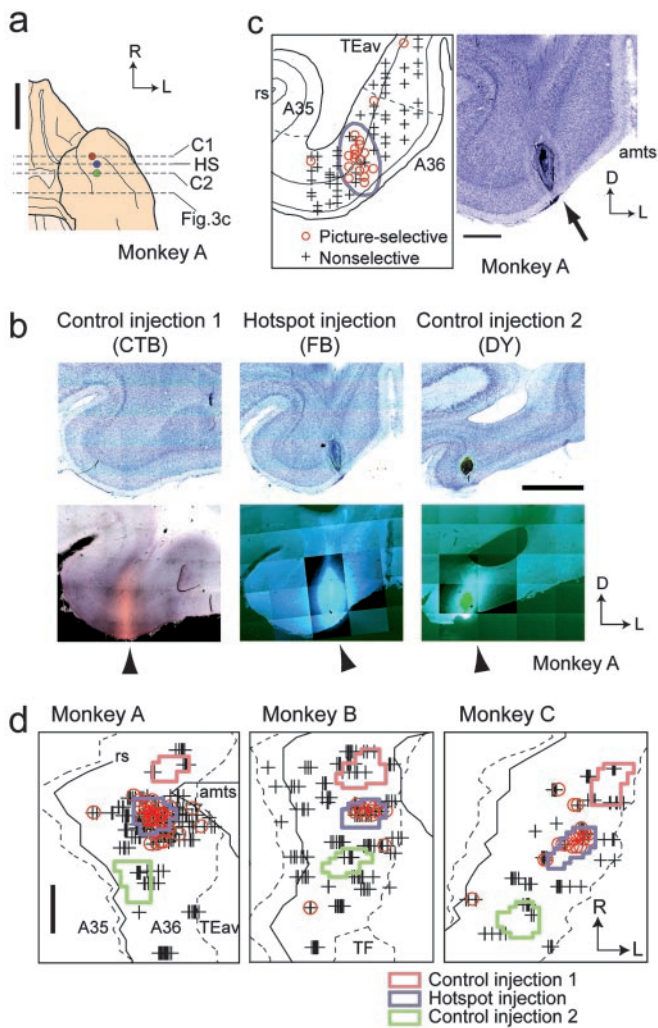
Fig. 2. Single-unit recording and tracer injection in A36. (*a*) Ventral view of a brain with an illustration of injection sites in A36. Circles show the locations of injection sites. Dotted lines denote the position of coronal sections containing injection sites displayed in *b* (HS, hotspot injection; C1 and C2, control injections) and the position of a section displayed in Fig. 3*c*. Data are for monkey A. (*b*) Bright-field (*Upper*) and dark-field (*Lower*) micrographs of coronal sections containing injection sites in A36. Arrowhead, injection site. The mosaic images were constructed by using a computerized microscope system. (*c*) A coronal section displaying the location of recorded neurons in A36 (*Left*) and the corresponding Nissl section (*Right*). Red circle, picture-selective neuron; gray cross, nonselective neuron; blue line, extent of the injection site; gray dotted line, border between A36 and TEav and border between A36 and A35; rs, rhinal sulcus; amts, anterior middle temporal sulcus; arrow, injection site. (*d*) Extent of injection to the hotspot (blue) and control injections sites (red and green). Symbols are the same as in *c*. Gray dotted line, border between A36 and adjacent areas; gray line, the lateral lip of the rs and the medial lip of the amts; TF, area TF; R, rostral; L, lateral; D, dorsal. [Scale bars: 10 mm (*a*), 2 mm (*b* and *d*), and 1 mm (*c*).]

tion sites were clearly visible on the coronal sections as a core of each tracer with surrounding nonneuronal cells (20) after the injection of fluorescent tracers (arrowheads in Fig. 2*b Center* and *Right*) and as a homogeneously stained brown region (19) after the injection of CTB (arrowhead in Fig. 2*b Left*). The identified injection site shows that the tracers were locally injected into the gray matter of A36 and that the tracers occupied most of the cortical layers (Fig. 2 *b* and *c*). The unfolded maps demonstrate that the tracers were injected, as targeted, into the hotspot (Fig. 2*d*, hotspot injection) and the regions adjacent to but outside the
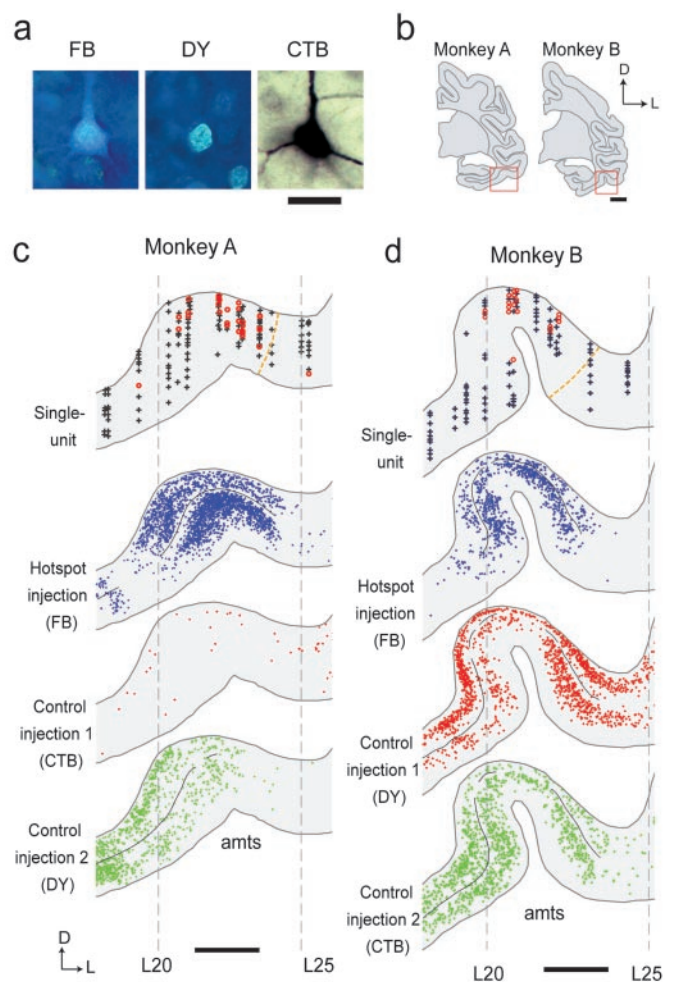

Fig. 3. Single-unit recording and retrograde labels in TEav. (*a*) Retrogradely labeled neurons in TEav. (*b*) Coronal sections including recording sites in TEav. Red rectangles denote the regions displayed in *c* and *d*. (*c* and *d*) The location of recorded neurons (upper image) and the distribution of retrograde labels (lower three images) in TEav of monkey A (*c*) and monkey B (*d*). In the single-unit recording display, data from four slices (≈1.6 mm) were superimposed. Symbols are the same as in Fig. 2*c*. In the retrograde labels display, data from two slices (≈0.8 mm) were superimposed. Each dot denotes a single retrogradely labeled neuron. Black lines in the depth of the layer IV denote the regions included as clusters. Note that the threshold for clusters was different between subjects and tracers. Gray dotted lines denote coordinates determined from x-ray imaging. L20, for example, denotes the line 20 mm lateral to the center. An orange dotted line denotes the border between TEav and the anterodorsal part of area TE. [Scale bars: 50 μm (*a*), 5 mm (*b*), and 2 mm (*c* and *d*).]

hotspot (Fig. 2*d*, control injection 1 and 2). The rostrocaudal diameter of the injection sites ranges 1.0–1.9 mm (mean 1.4 mm, *n* = 9). The distance between the center of the hotspot injection and the center of the control injection is 1.9–3.2 mm (mean 2.5 mm, *n* = 6).

Distribution of Picture-Selective Neurons and Retrograde Labeling in TEav. The distributions of recorded neurons and retrogradely labeled neurons were compared in TEav (Fig. 3). Of 1,189 recorded neurons in TEav, 262 were responsive and 232 were picture selective (ANOVA, $P < 0.01$; ref. 11). The correlation coefficient for paired pictures of the 232 neurons was significantly larger than zero (median = 0.14, $P < 0.001$, Wilcoxon signed-rank test) but much smaller than that of A36 picture-selective neurons (median value = 0.51, $P < 10^{-6}$; Kolmogorov–Smirnov test; ref. 11). Retrogradely labeled neurons in TEav

NEUROSCIENCE

(FB, DY, and CTB) are shown in Fig. 3a. The distribution of retrogradely labeled neurons and recorded neurons of two monkeys is shown in Fig. 3 c and d. TEav picture-selective neurons (red circles) were localized around the anterior middle temporal sulcus (Fig. 3 c and d, upper image). The distribution of retrograde labels at the same rostrocaudal level is also shown (Fig. 3 c and d, lower images). Neurons retrogradely labeled by the hotspot injection (defined as HS retrograde labels) and those labeled by the control injections (C1 or C2 retrograde labels) aggregated around the anterior middle-temporal sulcus, forming clusters of labels (Fig. 3 c and d). The clusters from different tracers were not segregated but partially overlapped. A comparison of the single-unit (Fig. 3 c and d, upper image) and retrograde labels (Fig. 3 c and d, lower images) revealed (i) that the regions in which TEav picture-selective neurons aggregated are included in the cluster of HS retrograde labels; and (ii) that within the cluster of HS retrograde labels, the regions with sparse C1 or C2 retrograde labels contained abundant picture-selective neurons in TEav.

To further quantify the above observations (i and ii), we compared two-dimensional unfolded maps of the density of retrograde labels in TEav (Fig. 4a) with the map of a single-unit recording (Fig. 4a; ref. 11). The regions densely labeled by the tracer were defined statistically as clusters in each retrograde label map (see *Supporting Methods*). In each of three retrograde label maps, two or three clusters were detected in TEav (Fig. 4a, white line). Densely labeled regions around the injection sites (Fig. 4a, purple line) were excluded from the analysis. Observation i was statistically tested by ROI-based analysis (see *Methods*): In each ROI (for example, the cluster of HS retrograde labels), the percentage of TEav picture-selective neurons was calculated. The percentage of TEav picture-selective neurons inside the clusters of the HS retrograde labels was significantly higher than that inside the clusters of the C1 or C2 retrograde labels in three monkeys ($\chi^2_1 = 9.0$, $P = 0.003$, HS retrograde labels vs. C1 retrograde labels; $\chi^2_1 = 40.7$, $P < 0.001$, HS retrograde labels vs. C2 retrograde labels; CMH test; Fig. 4b). This result confirmed observation i and demonstrated that the clusters of HS retrograde labels in TEav preferentially provide the task-related visual information to the hotspot in A36.

Next, we tested observation ii statistically. For this purpose, the clusters of HS retrograde labels were subdivided into two regions according to whether the region is included within the cluster of C1 or C2 retrograde labels (defined as HS-label-overlapping) and another that is not included (defined as HS-label-only; Fig. 4c). The percentage of TEav picture-selective neurons was significantly higher in the HS-label-only region than in the HS-label-overlapping region ($\chi^2_1 = 11.5$, $P < 0.001$; CMH test; Fig. 4c), confirming observation ii.

Fine Structure Within Clusters of HS Retrograde Labels. The result in Fig. 4c demonstrates that the HS-label-only region contains more abundant TEav picture-selective neurons than does the HS-label-overlapping region. By definition, the HS-label-only region projects less divergently to the hotspot in A36 than does the HS-label-overlapping region. Thus, these two lines of evidence indicate that the region containing abundant TEav picture-selective neurons (HS-label-only region) projects less divergently to the hotspot in A36. This finding raises a possibility that the TEav picture-selective neurons themselves project less divergently to the hotspot than do the TEav nonselective neurons. To test this possibility, we compared the degree of divergent projection between TEav picture-selective and TEav non-selective neurons by defining DI (Fig. 5a and *Methods*). If the DI of a pixel is high, then neurons in the pixel project less divergently to the hotspot injection site. A correlation analysis based on Monte Carlo technique (see *Supporting Methods* and Fig. 7,
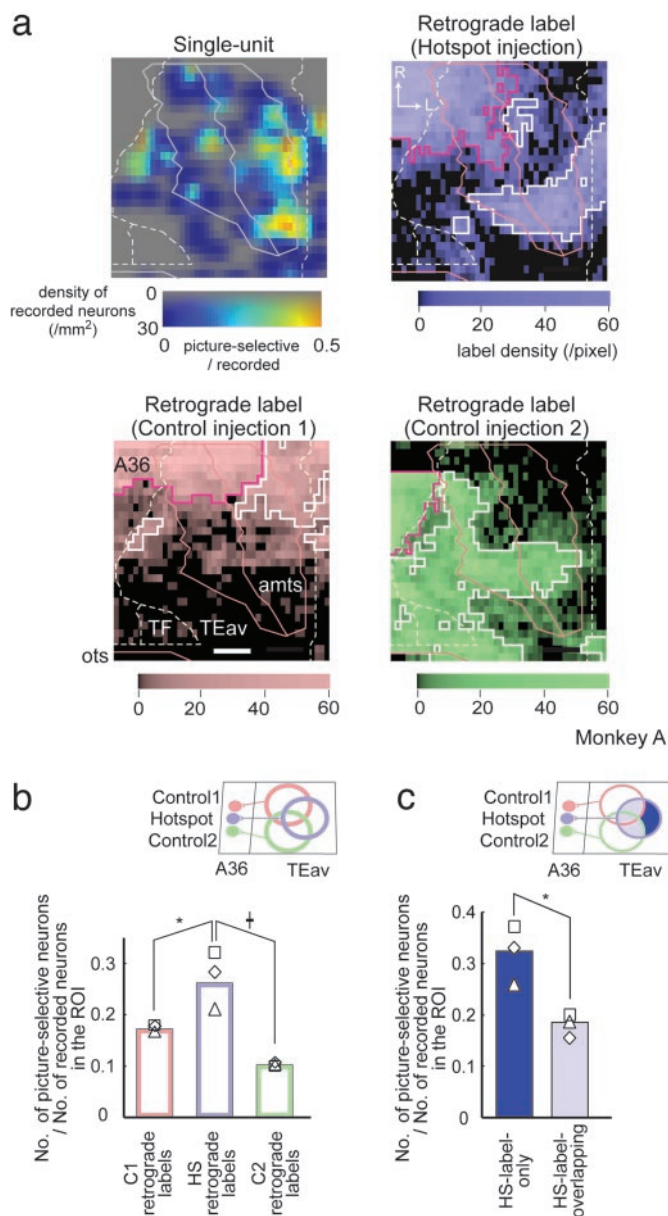

Fig. 4. A comparison of the distribution of retrogradely labeled neurons in TEav with that of picture-selective neurons. (a) Two-dimensional unfolded maps of single-unit and retrograde labels (hotspot injection, control injection 1 and 2). In the single-unit map, the saturation of the color bar denotes the density of recorded neurons and the hue denotes the number of picture-selective neurons per pixel/the number of recorded neurons per pixel. In retrograde-label maps, the density of retrograde labels is color-coded. White line, pixels defined as clusters; purple line, densely labeled pixels near the injection site (see *Supporting Methods*). Borders and sulci are shown in lines. Data are for monkey A. (Scale bar: 2 mm.) (b and c) the number of picture-selective neurons in the ROI/the number of recorded neurons in the ROI. In b, the ROIs are clusters of the C1 retrograde labels, the HS retrograde labels, and the C2 retrograde labels, respectively. In c, the ROIs are the region outside (HS-label-only) and inside (HS-label-overlapping) the clusters of C1 or C2 retrograde labels. Each symbol denotes the value of each monkey ($\diamond$, monkey A; $\square$, monkey B; and $\triangle$, monkey C). b: *, $P < 0.005$; †, $P < 0.001$. c: *, $P < 0.001$.

which are published as supporting information on the PNAS web site, for further details) demonstrated that the map of the percentage of TEav picture-selective neurons (Fig. 5b Center) was spatially correlated with the DI map (Fig. 5b Left; $r = 0.38$, $P < 0.05$). In the other two monkeys, the maps were also spatially correlated ($r = 0.30$ and 0.17, $P < 0.05$ in both monkeys).
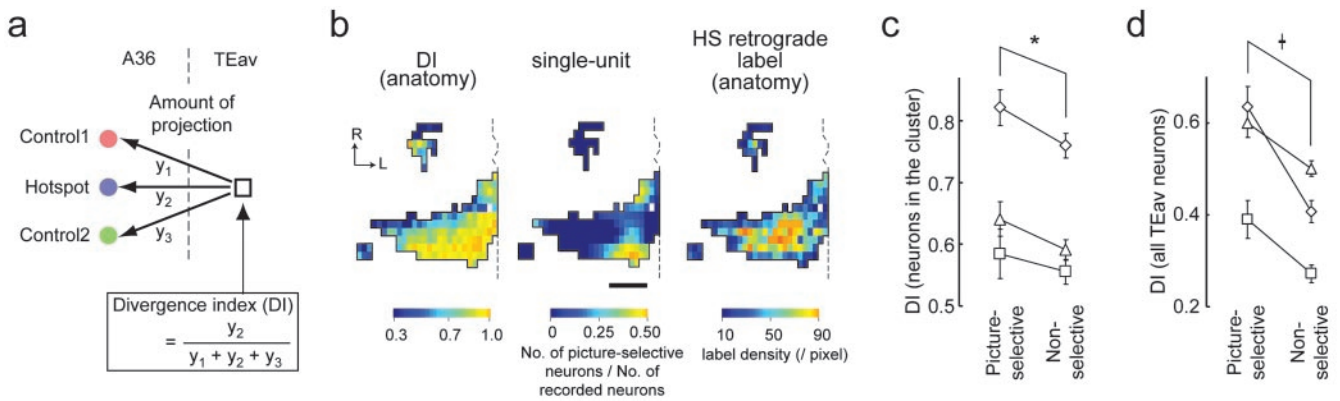
Fig. 5. Analysis using DI is shown. (*a*) Calculation of DI. Amount of the projection from neurons in a TEav pixel (right square) to three injection sites (left circles) is expressed as y_1, y_2, and y_3 (control injection 1, hotspot injection, and control injection 2, respectively). DI was defined as $y_2/(y_1 + y_2 + y_3)$. (*b*) A map of DI (*Left*), a single-unit map (*Center*), and a map of the density of HS retrograde labels (*Right*). Color bars show the value of each pixel. Data are for monkey A. (Scale bar: 2 mm.) (*c* and *d*) The DIs of TEav neurons in the cluster of HS retrograde labels (*c*) and of all recorded TEav neurons (*d*) were compared between picture-selective neurons and nonselective neurons. The mean value and standard error for each monkey are expressed as symbols and error bars. The symbols denote the same monkeys as Fig. 4*b*. *, $P < 0.02$; †, $P < 0.001$.

These observations were confirmed by an analysis on a neuron-by-neuron basis: we assigned to each recorded neuron the DI that was linearly interpolated from DIs in the surrounding pixels and then the DI was compared between TEav picture-selective neurons and nonselective neurons (Fig. 5*c*). Two-way ANOVA (monkey × neuron type) indicated that the DI was significantly higher in TEav picture-selective neurons than in TEav nonselective neurons ($F_{1, 505} = 6.05$, $P = 0.014$, after logit conversion; Fig. 5*c*). There was no significant interaction between monkey and neuron type ($F_{2, 505} = 0.45$, $P = 0.63$). When the difference in the total number of retrograde labels was normalized (see *Methods*), the result also showed statistical significance ($F_{1, 505} = 6.39$, $P = 0.011$, after logit conversion) and the interaction between monkey and neuron type was not significant ($F_{2, 505} = 0.48$, $P = 0.62$). When the ANOVA was performed with all recorded TEav neurons, the result was the same as that for neurons inside the cluster ($F_{1,927} = 37.09$, $P < 0.001$, after logit conversion; Fig. 5*d*). All of these results indicate that picture-selective neurons in TEav project less divergently to the HS site than do nonselective neurons in TEav.

Because DI [$= y_2/(y_1 + y_2 + y_3)$] is a function of the density of HS retrograde labels ($= y_2$), we examined a possibility that the high DI in the TEav picture-selective neurons (Fig. 5*c*) might simply reflect a high density of HS retrograde labels. However, a comparison of maps indicates that the pixels with the highest percentage of TEav picture-selective neurons (Fig. 5*b Center*) did not coincide with the pixels with the highest density of HS retrograde labels (Fig. 5*b Right*). These two maps were not spatially correlated ($r = 0.04$, -0.11, and -0.02 in monkeys A–C, respectively). Moreover, two-way ANOVA indicated that the density of HS retrograde labels was not higher in TEav picture-selective neurons than in TEav nonselective neurons (see Fig. 8, which is published as supporting information on the PNAS web site, for further details). Thus, the above possibility was rejected. It should also be noted that a scheme that the response property of A36 neurons was determined solely by a simple summation of input from TEav and by a global topographical pattern of connectivity from TEav to A36 will predict that the regions with the highest percentage of picture-selective neurons coincide with the regions with the highest density of HS retrograde labels. Because this was not the case (Fig. 5*b Center* and *Right*), the above scheme cannot explain our results.

Distribution of Double-Labeled (DL) Neurons. The distribution of DL neurons (neurons labeled with both FB and DY) directly indi-

cates the distribution of TEav neurons projecting divergently to both the hotspot injection site and the control injection sites. The analysis of DL neurons provided further evidence that picture-selective neurons in TEav project less divergently to the hotspot injection site. See Fig. 9, which is published as supporting information on the PNAS web site, for further details.

Discussion

In this study, we trained monkeys to learn the pair-association memory task and characterized the connectivity that provides visual information from TEav to memory-coding neurons in A36. We found that TEav neurons selective to learned pictures project less divergently to the hotspot injection site in A36 where memory-coding neurons aggregate, than do nonselective neurons in TEav (Figs. 4, 5, and 9). This result demonstrates that the morphological difference, that is, the difference in the degree of divergent projection, is coupled to the physiological difference between neurons selective to learned pictures and nonselective neurons. The selective and nonselective neurons share similar properties in that they project to the hotspot injection site and that they likely provide visual information to the hotspot in A36 (see below). Thus, the physiological difference between these neurons indicates whether these neurons participate in the transmission of task-related visual information to the hotspot in A36. Therefore, we conclude that the morphological difference is coupled to the involvement of task-related visual processing. The present study demonstrates that this coincidence between
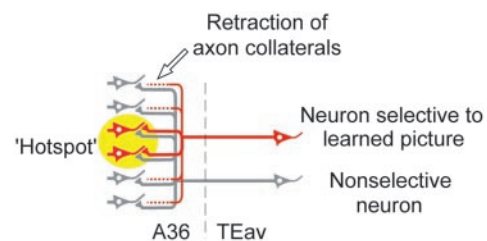

Fig. 6. A proposed scheme explaining the morphological basis of the reduced divergent projection found in this study. After extensive visual learning, fiber terminals projecting outside the hotspot were retracted in neurons selective to learned pictures (red). On the other hand, fiber terminals of nonselective neurons (gray) retained their divergence. The yellow circle denotes the hotspot in A36.

the morphological difference and the physiological difference is found consistently among all monkeys.

A caveat for the above discussion is that neurons selective to learned pictures and nonselective neurons may differ in physiological aspects other than their involvement in task-related visual processing. However, although most of the TEav neurons classified as nonselective were unresponsive to the learned pictures, these neurons are likely to be visually responsive. The visual responsiveness of TEav neurons is well established from previous studies. Anatomically, TEav is a unimodal association cortex (1, 2). Baylis *et al.* (17) showed in a single-unit study that TEav neurons are exclusively responsive to visual stimuli. Tamura and Tanaka (24) reported that at least 79% of neurons recorded in TEav are responsive to object images. Thus, the physiological difference between selective and nonselective neurons lies in whether they are involved in task-related visual processing.

Observations in the present retrograde labeling study are consistent with those in previous anatomical studies. Strong connections from TEav to A36 have been reported (12, 13). The partial overlap of retrograde labels for different tracers (Figs. 3 and 4) is consistent with previous reports on the divergent projection from TEav to A36 (12, 13). One of the findings in the present study is that the TEav region with dense picture-selective neurons projects specifically to the A36 region where memory-coding neurons were localized (Fig. 4*b*).

Previous electrophysiological studies demonstrate that structures similar to the hotspot emerge as a result of behavioral learning or experience (9, 10, 11, 25). Brain-derived neurotrophic factor (BDNF) mRNA is selectively induced in a focal patch within A36 during memory formation (26). Lesion studies

demonstrated a functional double dissociation where the PRh cortex is engaged in a mnemonic processing, whereas area TE is devoted to a perceptual processing (6, 7). Recently, we have found in a single-unit study that association between the representations of paired associates proceeds forward from area TE to A36 (11), which is consistent with the above lesion studies. The results of the present study, together with those of the studies cited above, support the view that forward signal transmission from area TE to A36 is the critical step from visual to mnemonic processing.

Considering all of the findings in this study, we speculate that the reduced divergent projection may be the result of the acquisition of visual long-term memory. One of possible schemes is that, after extensive visual learning, fiber terminals projecting outside the hotspot retract in TEav neurons selective to learned pictures, whereas fiber terminals of nonselective neurons retain their divergence (Fig. 6). Retraction of axon collaterals has been reported in development of the primary visual cortex (27, 28). Cortical map reorganization induced by lesions in adulthood (29–31) accompanies newly sprouted afferent terminals. Thus, the reduced divergent projection after learning found in the present study may share common mechanisms with cortical reorganization during development and/or regeneration.

1. Squire, L. R. & Zola-Morgan, S. (1991) *Science* **253,** 1380–1386.
2. Miyashita, Y. (1993) *Annu. Rev. Neurosci.* **16,** 245–263.
3. Zola-Morgan, S., Squire, L. R., Amaral, D. G. & Suzuki, W. A. (1989) *J. Neurosci.* **9,** 4355–4370.
4. Meunier, M., Bachevalier, J., Mishkin, M. & Murray, E. A. (1993) *J. Neurosci.* **13,** 5418–5432.
5. Murray, E. A., Gaffan, D. & Mishkin, M. (1993) *J. Neurosci.* **13,** 4549–4561.
6. Buckley, M. J., Gaffan, D. & Murray, E. A. (1997) *J. Neurophysiol.* **77,** 587–598.
7. Buffalo, E. A., Ramus, S. J., Clark, R. E., Teng, E., Squire, L. R. & Zola, S. M. (1999) *Learn. Mem.* **6,** 572–599.
8. Messinger, A., Squire, L. R., Zola, S. M. & Albright, T. D. (2001) *Proc. Natl. Acad. Sci. USA* **98,** 12239–12244.
9. Sakai, K. & Miyashita, Y. (1991) *Nature* **354,** 152–155.
10. Miyashita, Y. (1988) *Nature* **335,** 817–820.
11. Naya, Y., Yoshida, M. & Miyashita, Y. (2003) *J. Neurosci.*, in press.
12. Suzuki, W. A. & Amaral, D. G. (1994) *J. Comp. Neurol.* **350,** 497–533.
13. Saleem, K. S. & Tanaka, K. (1996) *J. Neurosci.* **16,** 4757–4775.
14. Higuchi, S. & Miyashita, Y. (1996) *Proc. Natl. Acad. Sci. USA* **93,** 739–743.
15. Naya, Y., Sakai, K. & Miyashita, Y. (1996) *Proc. Natl. Acad. Sci. USA* **93,** 2664–2669.
16. Naya, Y., Yoshida, M. & Miyashita, Y. (2001) *Science* **291,** 661–664.
17. Baylis, G. C., Rolls, E. T. & Leonard, C. M. (1987) *J. Neurosci.* **7,** 330–342.
18. Salin, P. A., Girard, P., Kennedy, H. & Bullier, J. (1992) *J. Comp. Neurol.* **320,** 415–434.
19. Luppi, P. H., Fort, P. & Jouvet, M. (1990) *Brain Res.* **534,** 209–224.
20. Conde, F. (1987) *J. Neurosci. Methods* **21,** 31–43.
21. Kulldorff, M. & Nagarwalla, N. (1995) *Stat. Med.* **14,** 799–810.
22. Besag, J. & Newell, J. (1991) *J. R. Stat. Soc. A* **154,** 143–155.
23. Mantel, N. & Haenszel, W. (1959) *J. Natl. Cancer Inst.* **22,** 719–748.
24. Tamura, H. & Tanaka, K. (2001) *Cereb. Cortex* **11,** 384–399.
25. Erickson, C. A., Jagadeesh, B. & Desimone, R. (2000) *Nat. Neurosci.* **3,** 1143–1148.
26. Tokuyama, W., Okuno, H., Hashimoto, T., Xin Li, Y. & Miyashita, Y. (2000) *Nat. Neurosci.* **3,** 1134–1142.
27. Antonini, A. & Stryker, M. P. (1993) *Science* **260,** 1819–1821.
28. Borrell, V. & Callaway, E. M. (2002) *J. Neurosci.* **22,** 6682–6695.
29. Darian-Smith, C. & Gilbert, C. D. (1994) *Nature* **368,** 737–740.
30. Buonomano, D. V. & Merzenich, M. M. (1998) *Annu. Rev. Neurosci.* **21,** 149–186.
31. Sur, M. & Leamey, C. A. (2001) *Nat. Rev. Neurosci.* **2,** 251–262.